

# End-to-end Cloud Segmentation in High-Resolution Multispectral Satellite Imagery Using Deep Learning

Giorgio Morales, Alejandro Ramírez, Joel Telles

National Institute of Research and Training in Telecommunications (INICTEL-UNI)

National University of Engineering, Lima, Peru

Email: giorgiomoralesluna@gmail.com

**Abstract**—Segmenting clouds in high-resolution satellite images is an arduous and challenging task due to the many types of geographies and clouds a satellite can capture. Therefore, it needs to be automated and optimized, specially for those who regularly process great amounts of satellite images, such as governmental institutions. In that sense, the contribution of this work is twofold: We present the CloudPeru2 dataset, consisting of 22,400 images of  $512 \times 512$  pixels and their respective hand-drawn cloud masks, as well as the proposal of an end-to-end segmentation method for clouds using a Convolutional Neural Network (CNN) based on the Deeplab v3+ architecture. The results over the test set achieved an accuracy of 96.62%, precision of 96.46%, specificity of 98.53%, and sensitivity of 96.72% which is superior to the compared methods.<sup>1</sup>

**Index Terms**—Cloud segmentation, end-to-end learning, satellite image.

## I. INTRODUCTION

Since the very beginning of remote sensing, clouds represents the most overwhelming type of noise in optical satellite imagery because it blocks everything beneath them. On the other hand, the high variance in its spectral response could add statistical noise into a database if some of its pixels get into it. For those reasons, filtering clouds through a detection process is one of the most traditional problems in remote sensing.

In the literature, this problem has been addressed from many perspectives; from empirical thresholded decision trees [1], [2], fuzzy logic [3], time series (if data available) [4], and machine learning [5]–[7] to a more recent approach: deep learning [8]–[10]. Even though some of the previous works achieved outstanding results, due the high risk that clouds represents, generating more accurate models for clouds detection is still valuable to enhance the results of deeper remote sensing methods/algorithms.

Due to the fact that some institutions, such as the National Commission for Aerospace Research and Development (CONIDA) of Peru, process a great number of satellite images daily, it is necessary to develop a method to automatically and rapidly obtain their correspondent cloud masks. For this,

<sup>1</sup>This paper is a preprint (submitted to the INTERCON 2019 conference, Lima, Peru). IEEE copyright notice. 2019 IEEE. Personal use of this material is permitted. Permission from IEEE must be obtained for all other uses, in any current or future media, including reprinting/republishing this material for advertising or promotional purposes, creating new collective works, for resale or redistribution to servers or lists, or reuse of any copyrighted.

we propose an efficient cloud segmentation method for high-resolution multispectral satellite images using a trainable end-to-end convolutional neural network (CNN). In order to train our network and compare its performance with other methods, we propose a large dataset consisting of 22,400 image patches extracted from PERUSAT-1, a Peruvian satellite managed and supervised by CONIDA.

## II. PROPOSED METHOD

### A. CloudPeru2 Dataset

A PERUSAT-1 scene has four spectral bands: red (0.63-0.7 $\mu$ m), green (0.53-0.59 $\mu$ m), blue (0.45-0.50 $\mu$ m) and NIR (0.752-0.885 $\mu$ m). The spatial resolution of the multispectral bands is 2.8 m per pixel and that of the panchromatic band is 0.7 m per pixel.

We used 153 PERUSAT-1 scenes of variable sizes (from  $6176 \times 6012$  to  $12722 \times 9529$  pixels) and from different geographies to extract 2800 image patches of  $512 \times 512$  pixels and create the CloudPeru2 dataset [11]. The scenes were previously orthorectified and adjusted to reflectance values with atmospheric correction. Each image patch has a correspondent hand-drawn shadow mask. Image samples from the dataset are shown in Fig. 1. Nevertheless, for this work we used data augmentation to increase the dataset size in order to avoid overfitting problems. In that sense, we rotated each patch  $90^\circ$ ,  $180^\circ$  and  $270^\circ$ , and flipped horizontally each one so that we get a total of 22,400 patches. We split 90% of the data to create the training set, 5% to the validation set and 5% to the test set.

In a previous work [10], we presented the CloudPeru dataset, which was used to classify small image patches as clouds or non-clouds. This dataset consists of 476,422 image patches of  $27 \times 27$  pixels extracted from only 15 different PERUSAT-1 scenes. In contrast, the CloudPeru2 dataset presents a greater number of scenarios (e.g. snow and ocean) and a bigger patch size; besides, it was specifically created to solve a segmentation problem.

In order to appreciate and verify the diversity of scenarios of the CloudPeru2 dataset, we utilized t-SNE to sample the images by categories in a 2-D space, as shown in Fig. 2. For this, we used a small CNN of the same architecture as that of the network presented in [10], and we trained it in the

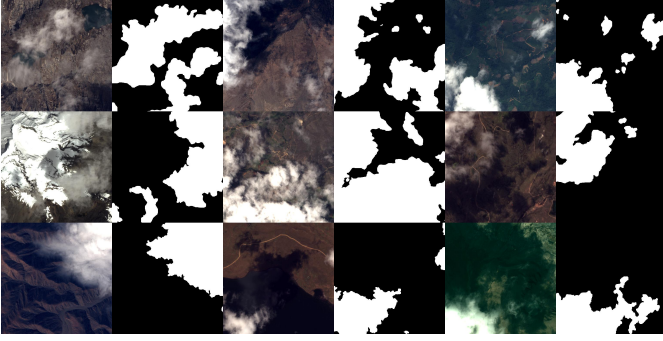


Fig. 1. Samples of original images and cloud masks from CloudPeru2 dataset.

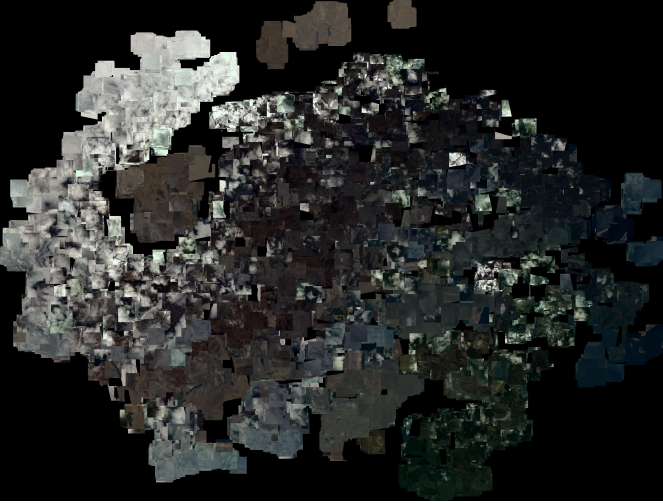


Fig. 2. Visualization of the CloudPeru2 dataset using t-SNE. Images fully covered by clouds are clustered in the left region. In the upper middle region are images of desert; below, snowy mountains and urban areas. Images of forest and ocean are clustered at the right.

SAT-6 airborne dataset [12]. Then, we resized the images of our dataset to  $27 \times 27$  pixels and used the trained network to extract a vector of 128 features (i.e. the output of the first fully connected layer ‘ $fc128$ ’) from them. Finally, the extracted feature vectors are mapped to the 2D space with t-SNE.

### B. Proposed CNN for Segmentation

We propose a semantic level segmentation of clouds in satellite imagery using a Convolutional Neural Network (CNN). The architecture of our network is the same as that used in [13] with the only difference that instead of three channels, our network uses inputs of four channels (R, G, B, and NIR). This CNN is based on the Deeplab v3+ architecture [14], which integrates an encoder, an atrous spatial pyramid pooling module (ASPP), and a decoder.

In Fig. 3 we show the proposed network architecture. Convolution blocks are denoted as “CONV;” inverted residual units, as “IRU;” and atrous separable convolution blocks, as “ASC”. The inverted residual unit (IRU) [15] expands the input number of channels using a  $1 \times 1$  convolution, then apply a  $3 \times 3$  depthwise convolution (the number of channels remains the same), and, finally, apply another  $1 \times 1$  convolution that reduces the number of channels. The atrous separable

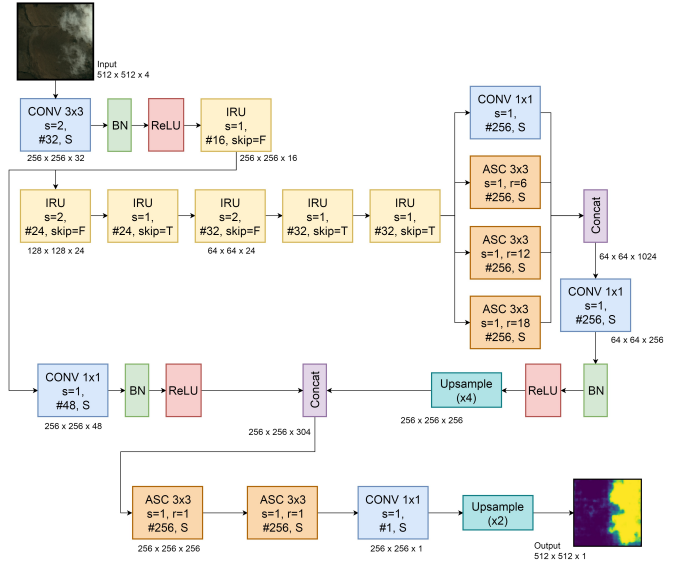


Fig. 3. The proposed network architecture. It uses regular convolutions (“CONV”), inverted residual units (“IRU”) and atrous separable convolutions (“ASC”).

convolution (ASC) is a depthwise convolution with atrous convolutions followed by a pointwise convolution. The output number of filters of each block is reported using the hash symbol (“#”). The stride of all convolutions is denoted as  $s$ . Blocks marked with S are same padded, which means that the output is the same size as the input. ReLU represents a standard rectified linear unit activation layer and BN a batch normalization layer.

## III. RESULTS

### A. Training Results and Metrics Comparison

The proposed algorithm was implemented using Python 3.6 on a server with Intel Xeon CPU E5-2620 at 2.1 GHz CPU, 128GB RAM and two NVIDIA GeForce GTX 1080 GPU. The proposed CNN was trained using an Adam optimizer with a learning rate of 0.003, a momentum term  $\beta_1$  of 0.9, a momentum term  $\beta_2$  of 0.999 and a mini-batch size of 8. Figure 4 shows the evolution of network accuracy and loss over 300 epochs.

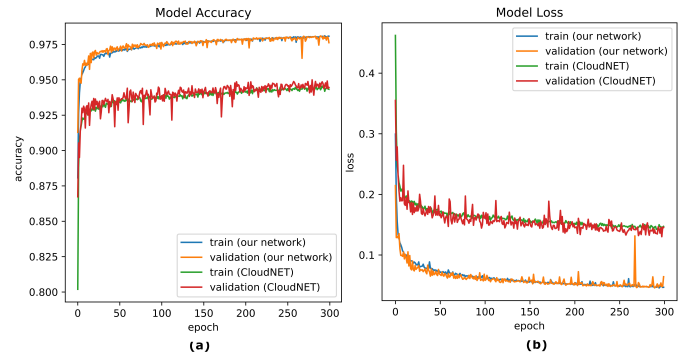


Fig. 4. Training and validation results of our method and CloudNet [16]. (a) Epochs vs. Accuracy (b) Epochs vs. Loss.

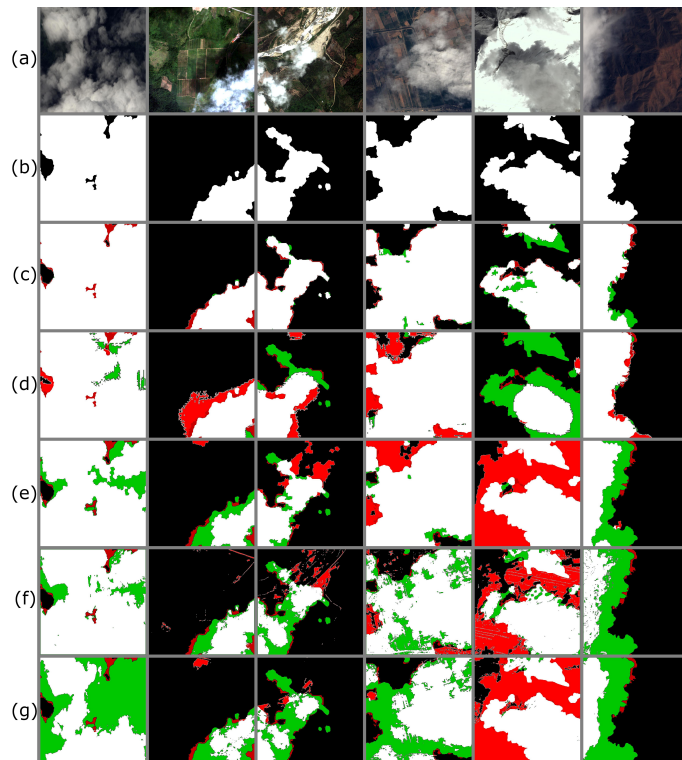


Fig. 5. Cloud segmentation using different methods. Green color represents False Negatives and red color, False Positives. (a) Original image (b) Ground truth (c) Our proposed method (d) CloudNet [16] (e) Method of [10] (f) Method of [7] (g) Progressive refinement.

In addition, we compared the ground truth with other four cloud detection methods. The first method [16] proposes a new deep residual architecture called CloudNet to semantically segment clouds. Its main unit uses a  $1 \times 1$  convolutional block of four channels followed by an ASPP module with seven dilation rates, whose results are concatenated along with the output of the first  $1 \times 1$  convolution. By doing so, it preserves the spatial information since it does not use any pooling or strided operation. We implement a network with 12 of these units, according to best achieved results reported by the authors. The second method [10] subdivides the image in superpixels, generates  $27 \times 27$ -pixel patches from each superpixel, and classifies each patch as cloud or non-cloud using a small CNN. The third method [7] calculates a set of texture and spectral descriptors and process them using a fully-connected neural network. Finally, the fourth method [17] uses a progressive refinement scheme.

We quantitatively compare all methods with respect to the ground truth using five metrics in the validation set: accuracy (ACC), precision (PREC), recall/sensitivity (SN), and specificity (SP), as shown in Table I. The ACC ratio indicates the correctly predicted observations against total observations; the PREC ratio indicates the correctly predicted positive observations against the total predicted positive observations; the SN ratio indicates the correctly predicted positive observations against the total actual positive observations, and the SP ratio indicates the correctly predicted negative observations against the total actual negative observations.

From Table I we observe that the greatest accuracy and sensitivity values correspond to our method (97.5% and 98.46%), evidencing a difference of more than three and eight percentage points, respectively, over CloudNET. The visual comparison of the cloud masks generated by all mentioned methods is shown in Fig. 5; these masks were generated from six different images with both low and high density clouds. It is observed that our method produces the most similar masks to the ground truth, specially when it comes to discern between snow and clouds (fifth column of Fig. 5), while other methods prioritize the segmentation of the most obvious high-density clouds. It is also worth mentioning that the most frequent type of error produced by our network is due to false positives, which can be proved by the fact that the lowest metrics of our network are the precision and specificity values; these errors are caused by small differences between the delineation of the borders of the ground truth and the generated masks. In the end, the results over the test set achieved an accuracy of 96.62%, precision of 96.46%, specificity of 98.53%, and

TABLE I  
METRICS COMPARISON OF DIFFERENT CLOUD DETECTION METHODS

Method	ACC (%)	PREC (%)	SN (%)	SP (%)
Prog. ref. [17]	89.41	82.50	80.72	90.25
ANN [7]	91.34	86.52	92.36	91.57
SLIC0 + CNN [10]	93.25	91.73	90.69	93.84
CloudNet [16]	94.01	<b>97.82</b>	89.78	<b>98.04</b>
Proposed method	<b>97.50</b>	96.45	<b>98.46</b>	96.58

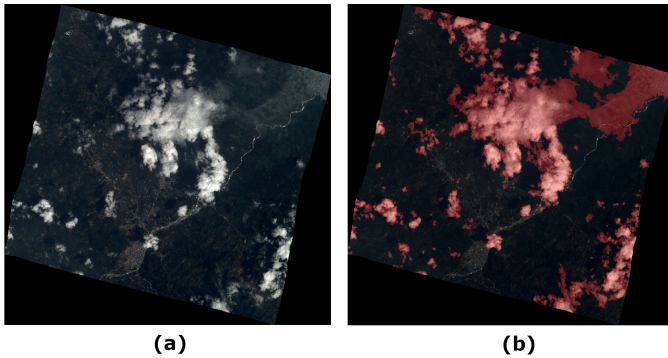


Fig. 6. Cloud segmentation result in a satellite scene with clouds of many sizes and densities. (a) Original PERUSAT-1 scene in RGB. (b) Segmented clouds are painted in red over the original image.

sensitivity of 96.72%.

We would also like to state that although our version of CloudNet has only 6,077 trainable parameters and our method has 503,377, the amount of computation and memory required by our approach is inferior than that of CloudNet. For instance, when training CloudNet, we had to reduce the number of training samples to just 15,960, use a mini-batch size of 12, and use randomly cropped images of  $200 \times 200$  in order to reduce the training time and memory consumption. This is explained by the fact that CloudNet does not reduce the size of its tensors at any moment, which consumes a lot of computational resources; while having small tensors with more number of channels consumes far less memory. Therefore, a single epoch for training our network (1330 batches, mini-batch size of 16, and inputs of  $512 \times 512$  pixels) lasted 20 minutes, while for training CloudNet (1330 batches, mini-batch size of 12, and inputs of  $200 \times 200$  pixels) lasted 22 minutes.

### B. Cloud Segmentation on Satellite Scenes

We have trained a CNN to segment clouds on small patches of  $512 \times 512$  pixels; however, the width and height of a PERUSAT-1 satellite scene are normally greater than 6000 pixels. Therefore, we move a  $512 \times 512$ -pixel sliding window across the scene in both horizontal and vertical direction with a 50-pixel overlap. In each position, we get a cloud probability mask using the trained network. In the overlapped areas, we consider the maximum probability value in order to avoid discontinuities in the final mask. Finally, we apply a threshold of 0.5 over the entire mask. Figure 6 shows the final cloud segmentation mask of a complete satellite scene.

## IV. CONCLUSIONS

In this paper, we propose an efficient method for segmenting clouds in high-resolution multispectral satellite images semantically. For this, we trained an end-to-end convolutional neural network based on a simplification of Google's Deeplab v3+ network. When comparing the results produced by our network with those produced by other cloud segmentation methods using the novel large dataset that we have proposed, we conclude that we achieved the best performance metrics. This method was embedded into a user-friendly interface used

by the National Commission for Aerospace Research and Development (CONIDA) of Peru, allowing them to process hundreds of satellite images automatically and rapidly.

## ACKNOWLEDGMENT

The authors would like to thank the National Commission for Aerospace Research and Development (CONIDA) and the National Institute of Research and Training in Telecommunications of the National University of Engineering (INICTEL-UNI) for the support provided.

## REFERENCES

- [1] Z. Zhu, and C. Woodcock, "Object-based cloud and cloud shadow detection in Landsat imagery," *Remote Sens. Environ.*, vol. 118, pp. 83-94, 2012.
- [2] A. Fisher, "Cloud and Cloud-Shadow Detection in SPOT5 HRG Imagery with Automated Morphological Feature Extraction," *Remote Sens.*, vol. 6, no. 1, pp. 776-800, 2014.
- [3] N. Singh, and A.A. Maxton, "Detection of Clouds and Cloud Shadow in Satellite Images using Fuzzy Logic," *Int. J. Advanced Res. Comp. Eng. Technol. (IJARCET)*, vol. 3, no. 4, pp. 1225-1228, 2014.
- [4] N. Champion, "Automatic Detection of Clouds and Shadows Using High Resolution Satellite Image Time Series," in *Int. Arch. Photogramm. Remote Sens. Spatial Inf. Sci. (ISPRS)*, Prague, 2016, pp. 475-479.
- [5] Y. Yuan and X. Hu, "Bag-of-words and object-based classification for cloud extraction from satellite imagery," *IEEE J. Sel. Topics Appl. Earth Observ. Remote Sens.*, vol. 8, no.8, pp. 4197-4205, 2015.
- [6] T. Bai, L. Deren, K. Sun, Y. Chen and L. Wenzhuo, "Cloud Detection for High-Resolution Satellite Imagery Using Machine Learning and Multi-Feature Fusion," *Remote Sensing*, vol. 8, no. 9, pp. 715, 2016.
- [7] G. Morales, S.G. Huamán and J. Telles, "Cloud Detection for PERUSAT-1 Imagery Using Spectral and Texture Descriptors, ANN, and Panchromatic Fusion," in *Proceedings of the 3rd Brazilian Technology Symposium - Emerging Trends and Challenges in Technology (BTSym17)*, Brazil, 2017, pp. 1-7.
- [8] M. Shi, F. Xie, Y. Zi and J. Yin, "Cloud detection of remote sensing images by deep learning," in *Proc. IEEE Int. Geosc. and Remote Sens. Symp. (IGARSS)*, Beijing, 2016, pp. 701-704.
- [9] M. Bartoš, "Cloud and Shadow Detection in Satellite Imagery," Master Thesis, Faculty Elect. Eng., Czech Tech. Univ. in Prague, Prague, 2017.
- [10] G. Morales, S.G. Huamán, and J. Telles, "Cloud Detection in High-Resolution Multispectral Satellite Imagery Using Deep Learning," in *Lect. Notes Comput. Sci.*, vol 11141, in *Proceedings of the 28th International Conference on Artificial Neural Networks (ICANN 2018)*, Greece, 2018, pp. 280-288.
- [11] G. Morales and A. Ramírez, CloudPeru2 Dataset. (2019) [Online]. Available: <http://didt.inictel-uni.edu.pe/dataset/CloudPeru2.zip>
- [12] S. Basu, S. Ganguly, S. Mukhopadhyay, R. Dibiano, M. Karki, and R. Nemani, "DeepSat - A Learning framework for Satellite Imagery", in *Proceedings of the 23rd SIGSPATIAL International Conference on Advances in Geographic Information Systems*, Seattle, Washington, 2015.
- [13] G. Morales, G. Kemper, G. Sevillano, D. Arteaga, I. Ortega, and J. Telles, "Automatic Segmentation of *Mauritia flexuosa* in Unmanned Aerial Vehicle (UAV) Imagery Using Deep Learning, *Forests*, vol. 9, no. 12, p. 736, Nov. 2018.
- [14] L.-C. Chen, Y. Zhu, G. Papandreou, F. Schroff, and H. Adam, "Encoder-Decoder with Atrous Separable Convolution for Semantic Image Segmentation," in *Proceedings of the European Conference on Computer Vision (ECCV 2018)*, in *Lect. Notes Comput. Sci.*, vol 11211, Munich, Germany, 2018.
- [15] M. Sandler, A. Howard, M. Zhu, A. Zhmoginov, and L.-C. Chen, "MobileNetV2: Inverted Residuals and Linear Bottlenecks," *arXiv* 2018. arXiv:1801.04381.
- [16] C.-C. Liu, Y.-C. Zhang, P.-Y. Chen, C.-C. Lai, Y.-H. Chen, J.-H. Cheng, and M.-H. Ko, "Clouds Classification from Sentinel-2 Imagery with Deep Residual Learning and Semantic Image Segmentation, *Remote Sensing*, vol. 11, no. 2, p. 119, 2019.
- [17] Q. Zhang, and C. Xiao, "Cloud Detection of RGB Color Aerial Photographs by Progressive Refinement Scheme," *IEEE Trans. Geosci. Remote Sens.*, vol. 52, no. 11, pp. 7264-7275, 2014.